Stokesian dynamics of close particles

Maria L. Ekiel-Jeżewska,[1] Tomasz Gubiec,[1,2] and P. Szymczak[3]
[1]*Institute of Fundamental Technological Research, Polish Academy of Sciences,
Świętokrzyska 21, 00-049 Warsaw, Poland*
[2]*Institute of Experimental Physics, Warsaw University, Hoża 69, 00-681 Warsaw, Poland*
[3]*Institute of Theoretical Physics, Warsaw University, Hoża 69, 00-681 Warsaw, Poland*

Stokesian dynamics simulations of close particles are reported, taking into account lubrication forces and many-body hydrodynamic interactions between spheres. A periodic trajectory of three particles maintaining a permanent proximity to each other has been found and analyzed. This solution is used as a benchmark to study the accuracy and stability of various numerical integration schemes. In particular, different methods of preventing unphysical overlaps of the particles are considered and potential artifacts discussed. © *2008 American Institute of Physics.*
[DOI: 10.1063/1.2930881]

I. INTRODUCTION

The paper is focused on hydrodynamic interactions between very close solid spheres moving in a viscous fluid at the low Reynolds number.[1,2] Hydrodynamic interactions influence significantly statistical properties of suspensions and, therefore, a lot of work has been done to analyze them theoretically[1] and to construct numerical codes suited for efficient and accurate computations, such as lattice Boltzmann[3] and Stokesian dynamics.[4,5] For dense systems, interaction between very close particle surfaces is essential. As the spheres approach each other at a very small distance, it becomes increasingly difficult to squeeze out the thin lubrication layer of fluid from in between them. The hydrodynamic lubrication forces associated with this motion[6] prevent the particles from touching each other. Lubrication of very close solid surfaces is hard to tackle numerically. In particular, due to the numerical errors in the finite-difference schemes, there is often a possibility of an unphysical overlap of the particles, which needs to be carefully avoided in the simulations. Several methods for assisting with this problem have been devised.[7–12] However, they introduce numerical artifacts, which may significantly influence the dynamics of the particles at short distances.[10,12,13] In this paper, we investigate these effects.

In a number of systems, motion of several spheres was detected experimentally or evaluated by the Stokesian dynamics, and some very close configurations of the spheres were observed, with the distance between the sphere surfaces smaller than 1% of the radius.[14–17] Many examples of "scattering processes" are known, during which very small gaps between the particle surfaces are reached and then particles separate again, for example, a sphere falls under gravity onto the other one held fixed or moving slower below.[14,15] The question arises if there exist stable systems of a different nature—with at least three spheres staying very close to each other for a long time, thus forming a "cluster" instead of moving quickly far away from each other.

In this paper, the Stokesian dynamics algorithm HYDRO-MULTIPOLE, based on irreducible multipole representation,[5,18]

is used to find and investigate a family of such "benchmark clusters," made of a small number of close particles, which settle under gravity. We study a periodic trajectory of three spheres, during which all of them remain in a close proximity of each other. Such a trajectory is ideally suited for testing various numerical schemes since—as it turns out—even small numerical errors or artifacts may result in significant changes of the observed period of the motion. Moreover, the oscillations of very close sedimenting triplets are also of fundamental physical importance.

In Sec. II, theoretical foundations of the Stokesian dynamics[5] and the numerical procedure[18] are outlined. Section III contains a brief review of methods used to integrate numerically the dynamics of very close spheres. In Sec. IV, the periodic motion of three very close spheres is analyzed. In Sec. V, this system is used to test selected numerical procedures, with the conclusions presented in Sec. VI.

II. DYNAMICS

Consider a system made of identical solid spheres of diameters d, which settle under gravitational forces $\mathbf{f}$ in a fluid of viscosity η. The spheres are close to each other, but their surfaces do not touch. The Reynolds number of the generated flow is much smaller than unity; therefore, the fluid velocity $\mathbf{u}$ and pressure p satisfy the Stokes equations,

$$\eta\nabla^2\mathbf{u} - \nabla p = \mathbf{0}, \tag{1}$$

$$\nabla \cdot \mathbf{u} = 0. \tag{2}$$

The no-slip boundary conditions are satisfied at the sphere surfaces. Positions of the sphere centers $\mathbf{r}_i$ evolve according to the following Stokesian dynamics equations:

$$\frac{d\mathbf{r}_i}{dt} = \mathbf{v}_i(\mathbf{r}_1, \mathbf{r}_2, \ldots, \mathbf{r}_N), \quad i = 1, 2, \ldots, N, \tag{3}$$

$$\mathbf{v}_i = \left[\sum_{k=1}^{N} \boldsymbol{\mu}_{ik} \right] \cdot \mathbf{f}, \tag{4}$$

where $\boldsymbol{\mu}_{ik}(\mathbf{r}_1, \mathbf{r}_2, \ldots, \mathbf{r}_N)$ are the N-particle translational-translational mobility matrices,[1,19] evaluated numerically by the multipole expansion of the Stokes equations. The algorithm from Ref. 5 and its precise numerical FORTRAN implementation HYDROMULTIPOLE described in Ref. 18 have been used with the multipole order $L=4$. To describe accurately dynamics of close spheres, lubrication correction has been applied according to the procedure taken from Ref. 18. For rigid-body motions, the relative accuracy of the mobility matrix is typically of the order of 0.01% for $L=4$ (see Ref. 5).

It is convenient to use $3N$-dimensional vectors of the particle positions and velocities and the forces exerted by them on the fluid, $\mathbf{X}=(\mathbf{r}_1, \mathbf{r}_2, \ldots, \mathbf{r}_N)$, $\mathbf{V}=(\mathbf{v}_1, \mathbf{v}_2, \ldots, \mathbf{v}_N)$, and $\mathbf{F}=(\mathbf{f}, \mathbf{f}, \ldots, \mathbf{f})$, respectively. In this notation, the system of Eqs. (3) and (4) reads

$$\frac{d\mathbf{X}}{dt} = \mathbf{V}(\mathbf{X}), \tag{5}$$

$$\mathbf{V} = \boldsymbol{\mu} \cdot \mathbf{F}. \tag{6}$$

The dimensionless variables are obtained by dividing positions by the sphere diameter d and time by twice the Stokes time,

$$\tau_s = 3\pi\eta d^2/f, \tag{7}$$

with $f=|\mathbf{f}|$. Therefore, velocities are normalized by the Stokes velocity $v_s = f/(3\pi\eta d)$. From now on, $\mathbf{r}_i$, $\mathbf{v}_i$, and t will denote the dimensionless quantities.

III. NUMERICAL INTEGRATION

In general, due to lubrication forces, the normal relative motion of the particle pair ij is strongly hindered as the dimensionless gap between them, $|\mathbf{r}_j - \mathbf{r}_i| - 1$, goes to zero. This effect prevents the particle contact during the evolution. However, when a finite time step is used in the numerical integration of the equations of motion, the particles may overlap. It is important to realize that it is a pure numerical artifact of the integrating routine. This problem was already noted in the literature and was dealt with in a variety of ways. One of the possibilities is to introduce a short-ranged repulsive potential to prevent the overlaps (see, e.g., Refs. 7, 9, and 11–13). A number of different potentials have been considered (e.g., inverse Hookean springs, power law, etc.). Interestingly, in some cases, the form and magnitude of the potential was found to significantly influence both the transport properties and the particle distribution function in the system.[12,13,17,20] Alternatively, in Refs. 17 and 21, the particles were allowed to overlap for a short period of time. However, the mobility matrix $\boldsymbol{\mu}$ is not defined for overlapping particles. To circumvent that difficulty, when the overlap is detected, the radii of the spheres are renormalized so that the smallest gap between the particles is equal to 10^{-8}.

Yet, another method was used by Ladd:[8] Reflect the particles elastically each time they are going to overlap. To be more precise, after calculating the particle velocities accord-

ing to Eq. (4), the hard-sphere dynamics is implemented over one time step: The possible collisions between the particles are located and then carried out, as described by Alder and Wainwright.[22] After the completion of the time step dt, the hydrodynamic mobility matrix $\boldsymbol{\mu}$ is calculated again, for the new particle positions $[\mathbf{X}(t+dt)]$, and then the procedure is repeated.

The overlap problem may be avoided by decreasing the time step as the spheres approach each other. One of such schemes was proposed by Ball and Melrose:[10] Given the set of velocities calculated from Eq. (4), they detected the potential overlaps and decreased the time step in such a way as to prevent them. However, if a method of this kind is used, there is a price to pay: Although the particles no longer overlap, the close encounters of the particles may involve very small time steps and, hence, a considerable amount of computer time. This is undesirable when simulating many-particle systems, such as concentrated colloidal suspensions in which close encounters of the particles occur frequently. In this context, it is worth exploring in more detail alternative ways of preventing particle overlaps in order to find a method that would be both acceptably fast and accurate. To assess the accuracy and effectiveness of the methods, there is a need for benchmark test system. Below, we propose such a benchmark trajectory, which involves three particles that remain constantly in close contact. A precise determination of the particle evolution along this trajectory constitutes a stringent test for the numerical methods since the potential artifacts introduced by numerical treatment of overlaps in this case will become amplified in the course of time.

IV. PERIODIC MOTIONS OF VERY CLOSE SPHERES

In a number of systems, gravitational settling of a group of spheres has been detected experimentally[23] or evaluated by the Stokesian dynamics,[24,25] and a generic "scattering" pattern of evolution has been found: Initially, well-separated particles approach each other, interact for some time, and separate again. The evolution can be very sensitive to a small change of the initial conditions.[25] Such a scenario sometimes involves very close configurations of the spheres, with the distance between the sphere surfaces smaller than 10^{-2} radii, for example, when a sphere falls under gravity onto the other one held fixed or moving slower almost exactly below.[14,15] The particles stay close to each other, but for a short time only, and later on the interparticle distances grow indefinitely.

To test Stokesian dynamics at small separations between the particle surfaces, solutions of a different nature are needed: With a small number of nontouching spheres, which would move with respect to each other but stay very close for a long time. (Two identical spheres settle under gravity with no change of the relative configuration: Therefore, the simplest benchmark consists of three identical spheres.) Moreover, the particles should not change significantly their evolution under a small perturbation of the configuration. Therefore, an ideal benchmark would be a periodic trajectory of close spheres.

Periodic oscillations of three settling particles are known from the literature, but for well-separated surfaces. The first experimental evidence[23] and theoretical derivation within the point-particle approximation[24] were followed by extended mathematical analysis of periodic solutions for points[26] and by investigation of periodic solutions for spherical particles.[27]

In this work, we have found and analyzed periodic motion of three identical spheres settling under gravitational forces **f**, with at least two very small gaps between their surfaces at a time. Actually, we have found a class of quasi-periodic solutions with two incommensurate frequencies of oscillations. They surround a single-frequency solution, which will now be presented.

The z axis is chosen antiparallel to the gravitational force $\mathbf{f}=(0,0,-f)$, with $f>0$. The motion takes place in a vertical plane $y=0$. Positions of the sphere centers are denoted as $\mathbf{r}_i=(x_i,0,z_i)$, $i=1,2,3$, and positions and velocities of the center of mass as $\mathbf{r}_{CM}=(x_{CM},0,z_{CM})$ and $\mathbf{v}_{CM}=(v_{x,CM},0,v_{z,CM})$, respectively.

The initial positions of the sphere centers, corresponding to the single-frequency solution, are

$$x_1=-x_3\approx 0.626\,266,$$

$$z_1=-z_3\approx -0.779\,612, \tag{8}$$

$$x_2=z_2=0.$$

Therefore, initially, the sphere centers are aligned, with two equal interparticle distances, $|\mathbf{r}_1-\mathbf{r}_2|\equiv r_{12}=r_{23}$, corresponding to narrow gaps $r_{12}-1\approx 2\times 10^{-6}$ between the sphere surfaces. This configuration is shown in the first frame of Fig. 1.

Equations (3), (4), and (8) have been integrated with the adaptive Runge–Kutta (ARK) method with the required error density per unit time, $\rho=10^{-10}$ (for the definition of ρ, see Appendix A). With such a small error density, no overlaps have been observed. Accuracy of the numerical integration was estimated by comparing the trajectories with those evaluated by a more precise ARK routine with $\rho=10^{-13}$. After one period, the difference between values of r_{12} computed by these two procedures was of the order of 1×10^{-8} only.

The solution of the dynamics given by Eqs. (3), (4), and (8) is a superposition of a periodic motion with the period $T\approx 170$, and the gravitational settling with the time-averaged velocity,

$$\mathbf{V}=\frac{1}{T}\int_0^T \mathbf{v}_{CM}dt\approx -1.85\mathbf{e}_z. \tag{9}$$

Evolution of the system is illustrated in Fig. 1, as seen by an observer moving vertically with the time-averaged ve-

locity **V** and taking snapshots at the subsequent time instants separated by $T/36$. Two characteristic symmetric configurations of the spheres are observed. In the first one, seen at $t=0$ and then every $T/6$, the centers are aligned at the angle $\theta\approx 39°$ with respect to gravity, with the equal sizes of both gaps between the particle surfaces. In the second configuration, which appears at $t=T/12$ and later after each $T/6$, the sphere centers form an isosceles triangle with a vertical base, not much different from the equilateral one. The generic pattern of the evolution during $T/6$, depicted in Fig. 1, is then repeated, with the corresponding interchange of the particles, and the left-right symmetry between the configurations at t and $t+T/6$.

As shown in Fig. 1, the center of mass oscillates while settling, with the dominant horizontal component. The horizontal velocity is the largest for the first and the last snapshots of Fig. 1, i.e., for the aligned particles, see also Fig. 2. In this case, the sideways motion can be understood by analogy with two settling spheres or an oblique rod.[28,29]

The explicit time dependence of $\mathbf{v}_{CM}$ is shown in Fig. 2, where the horizontal and vertical components of the center-of-mass velocity are plotted as functions of time, in the frame settling vertically with the time-averaged velocity **V**. Note that the center-of-mass motion is characterized by the period equal to $T/3$ rather than T.

The time dependence of $v_{z,CM}$ indicates that vertical settling is the fastest for the almost equilateral configuration of the sphere centers seen at the middle snapshot of Fig. 1, i.e., at $t=T/12$, and then after every $T/6$. On the other hand, settling is the slowest for the configurations close to (but not exactly equal to) the second and the last but one snapshot, i.e., close to $T/36$ and $t=5T/36$, and then every $T/6$ after these time instants. For such configurations, the gaps between the particle surfaces are still larger than the minimal value, as shown in Fig. 3. The minimum of the interparticle distances is reached for only one pair of the spheres at a time and it is as small as 3.5×10^{-8}. Therefore, the logarithmic scale is used in Fig. 3 while plotting the distance between the
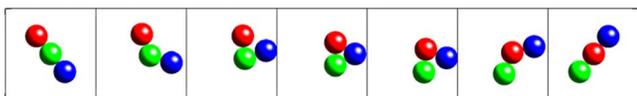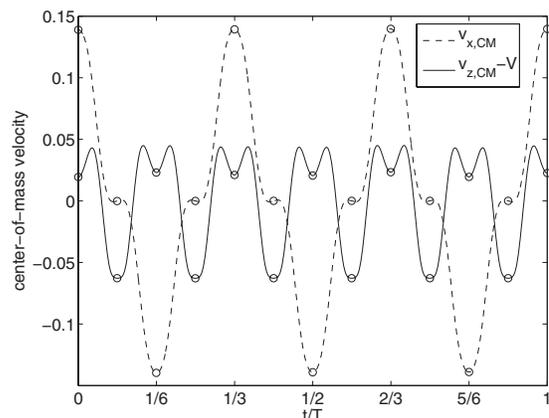

FIG. 1. (Color online) Configurations of the sphere centers at $t=T(n-1)/36$, with $n=1,2,\dots,7$, as seen by an observer settling vertically with the time-averaged velocity **V** given by Eq. (9).

FIG. 2. The instantaneous center-of-mass velocity as measured by an observer settling with the time-averaged velocity V. The symbols ○ denote the positions at every $T/12$.
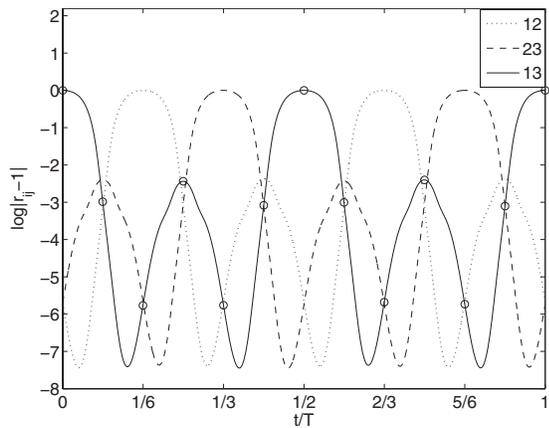
FIG. 3. The decimal logarithm of the distance between the sphere surfaces. The symbols ○ denote values of $\log(r_{13}-1)$ at every $T/12$.
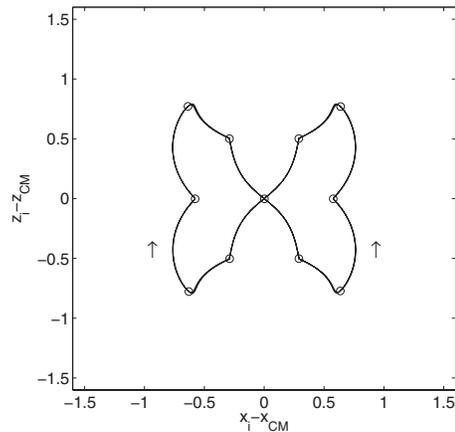

FIG. 5. The unique "butterfly" trajectory of all the sphere centers in the center-of-mass frame. The sense of the motion is indicated by the arrows. The symbols ○ denote the positions at every $T/12$ (enhanced online).

sphere surfaces $r_{ij}-1$ versus time. The minima are observed approximately at $T/30$ and $3T/10$, and every $T/6$ before and after these values. When the spheres are the closest to each other, their line of centers is almost (but not exactly) horizontal.

Trajectories of the centers of the spheres $z_i(x_i)$ and of the center of mass $z_{CM}(x_{CM})$ during a single period T are plotted in Fig. 4. It is worthwhile to subtract the settling motion and obtain closed trajectories of the sphere centers. One possibility is to adopt the center-of-mass frame. The corresponding trajectories, z_i-z_{CM} vs x_i-x_{CM}, are plotted in Fig. 5, with the corresponding movie linked online. A striking feature is that we obtain the same closed trajectory for all spheres. The particles circle along it separated by $T/3$. Existence of periodic solutions for the relative motion of three identical spheres in a fluid, chasing each other with a delay of one-third of a period like "ponies on a merry-go-round," have been mathematically predicted in Ref. 26, but no example has been described. Solutions of the same nature have been also found in a different context: For a self-gravitating system of three equal masses, which move along the same trajectory, a circle or a figure-eight curve.[30–32] The "butterfly"

shape of the trajectory shown in Fig. 5 is of a special interest also because of the existence of cusps—points, where the motion rapidly changes direction.

An alternative description of the relative motion is to use the relative coordinates of the sphere centers, $\mathbf{r}_{ij}=(x_{ij},0,z_{ij})$. The resulting trajectory, $z_{23}(x_{23})$, identical to $-z_{13}(x_{13})$, is plotted in Fig. 6. Surprisingly, this curve contains tips—the turning points, where the direction of the relative motion is reversed.

The motion of the sphere centers with respect to the center of sphere 3 is shown in the movie linked online. This movie illustrates that, most of the time, the shearing motion of the surfaces dominates the squeezing one. In Fig. 7, both squeezing v_n and shearing v_t components of the relative velocity $\mathbf{v}_{23}$ are plotted versus time. Indeed, the squeezing component v_n is negligible most of the time. The important observation is that at the smallest interparticle distances, the particle relative motion is practically restricted to the sliding only.[33] Moreover, rapid changes of v_n from/to zero correspond to significant changes of the direction of the relative
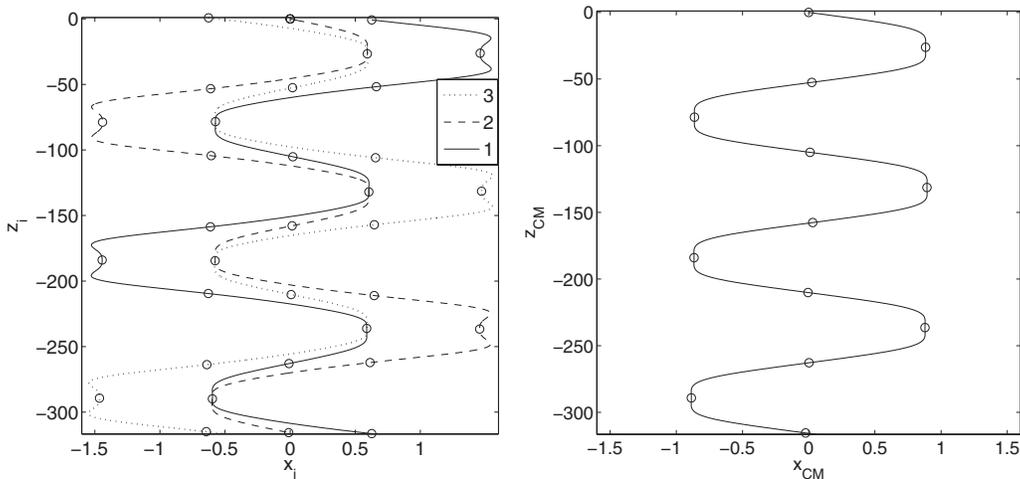

FIG. 4. Trajectories of the sphere centers (left) and of their centers of mass (right) in the laboratory frame. One period $T \approx 170$ is shown. The symbols ○ denote the positions at every $T/12$.
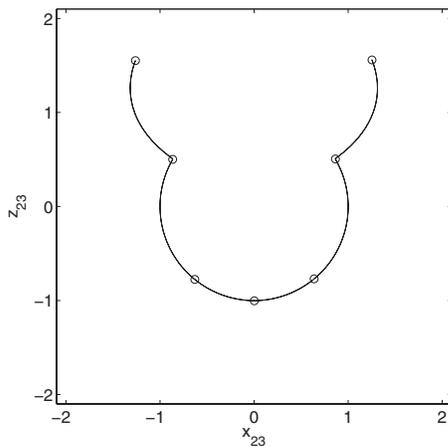
FIG. 6. The relative trajectory of the sphere centers. The positions are denoted by ○ at every $T/12$ (enhanced online).

FIG. 8. Spectral density Φ (square of the magnitude of the Fourier transform) of $x_2(t)$, i.e., the horizontal coordinate of a particle as a function of time. Top: The optimal trajectory with initial conditions given by Eq. (8). Bottom: A slightly perturbed trajectory with respect to the optimal one. The spectral density $\Phi(f)$ was normalized to one at the maximum.

motion, observed at the cusps and tips of the relative trajectory in Fig. 6.

With three dimensional numerical codes, we did not observe separation of the particles nor a change of the periodic benchmark solution even after 100 periods. The periodic solution presented above is robust, although it slowly moves out of the vertical plane and eventually the particles separate, if an off-plane perturbation is applied. On the other hand, if the "optimal" initial conditions (8) are slightly perturbed within the plane, the particles still oscillate, but quasiperiodically, with a second additional frequency. Such a behavior is generic even for such a symmetric initial configuration of the particle centers as the equilateral triangle with a vertical base. For example, for the size of its side equal to 1.01, the spectral density of $x_2(t)$ was computed and plotted in Fig. 8, side by side with the spectral density corresponding the optimal solution.

The frequency f_1 corresponds to the period of oscillations of the relative motion ($T \approx 170$ for the optimal trajectory), whereas the frequency $f_2 = 3f_1$ corresponds to the oscillations of the center of mass of the system (cf. Fig. 1). Finally, the smallest peak (f_3) on the bottom panel corre-
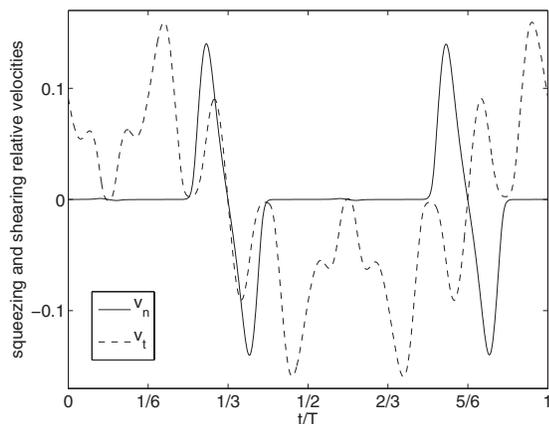

FIG. 7. Evolution of the squeezing and shearing components of the relative velocity, $v_n = \mathbf{v}_{23} \cdot \hat{\mathbf{n}}$ and $v_t = \mathbf{v}_{23} \cdot \hat{\mathbf{t}}$, with $\hat{\mathbf{n}} = \mathbf{r}_{23}/r_{23} = (\sin\theta, 0, \cos\theta)$ and $\hat{\mathbf{t}} = (\cos\theta, 0, -\sin\theta)$.

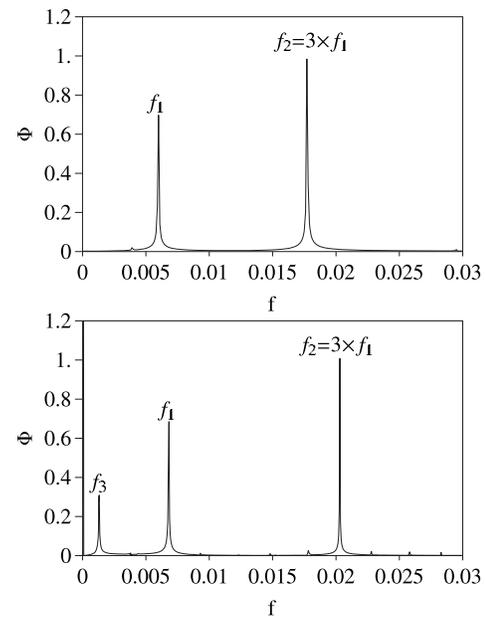sponds to the slow modulation around the periodic orbit. This modulation is inherent to the motion of the center of mass. For the solutions analyzed in Fig. 8, the corresponding plots of the spectral density of $x_2 - x_{CM}$ contain only the single peak f_1, and the plot of the spectral density of x_{CM}, only peaks f_2 and f_3 for the perturbed trajectory. Note that the positions of the peaks on both panels do not coincide, which shows that the period of the motion changes as the trajectory is perturbed.

V. TESTING INTEGRATION SCHEMES

In this section, we analyze influence of integration routine and the method of avoiding overlaps on the sphere dynamics. As a benchmark problem for assessing the accuracy and the efficiency of various numerical schemes, we use the periodic motion of three spheres described in the previous section, with the initial conditions given by Eq. (8). This gives a possibility to monitor such characteristics as the period or the minimal distance between the sphere surfaces on the trajectory, depending on the method.

As discussed in the previous section, the benchmark trajectory has been evaluated very precisely by the adaptive Runge–Kutta, ARK, method with the required error density per unit time, $\rho = 10^{-10}$. With such a small error density, no overlaps have been observed and the accuracy of the interparticle distance after a single period has been estimated as 1×10^{-8}.

Here, we compare this trajectory with the results obtained by various numerical algorithms used to integrate Eqs. (5) and (6). In each of them, we apply the same procedure to evaluate the mobility matrix, following Sec. II. As mentioned in Sec. III, finite time-step methods can lead to nonphysical overlapping of spheres, and additional procedures that pre-

vent this artifact are necessary. Adaptive routines can avoid that problem, but they slow down when the spheres approach each other and the timestep is decreased to very small values.

We consider two alternative ways of avoiding overlaps in the fixed timestep methods, i.e., the elastic collision method and radius renormalization method, as outlined in Sect. III. Those are incorporated into three integration schemes: Fourth order Runge–Kutta method (RK), fourth order Adams–Bashforth (AB) predictor method, and implicit Euler (IE) technique (described in Appendix B). This makes six different possibilities (IEC, IER, RKC, RKR, ABC, and ABR), depending on the choice of the integration scheme (IE, RK, and AB) and the overlap-avoiding method (collisions "C" or renormalization "R").

We also compare the above routines with the adaptive Runge–Kutta, ARK, integration scheme, supplemented by an additional time-step reduction by a factor of 2, if potential overlaps are detected. For the special case of the error density per unit time $\rho = 10^{-10}$, this procedure coincides with the benchmark routine discussed above, because no potential overlaps are detected.

Using less accurate routines is reasonable if they are faster than our reference method. To measure routine efficiency, we will use T_{CPU}, which is the time (in seconds) that CPU needs to calculate the system evolution during the time unit τ_s, defined in Eq. (7). For fixed time-step routines, T_{CPU} is almost constant during evolution. In the ARK method, time step decreases when spheres are closer to each other, so T_{CPU} should increase in such cases. Indeed, such a tendency can be observed in Fig. 9, where we plot the time dependence of T_{CPU} and of the smallest gap between the sphere surfaces,

$$\xi = \min(r_{12}, r_{23}, r_{31}) - 1. \tag{10}$$

The results obtained with different integration schemes are compared in Fig. 10 and Table I. For the fixed time-step routines, three values of the time step are used to control the convergence. For the ARK procedure, the time step is changing, but we can control the average time step $\langle dt \rangle$ by changing the error density per unit time ρ. For the data in Fig. 10
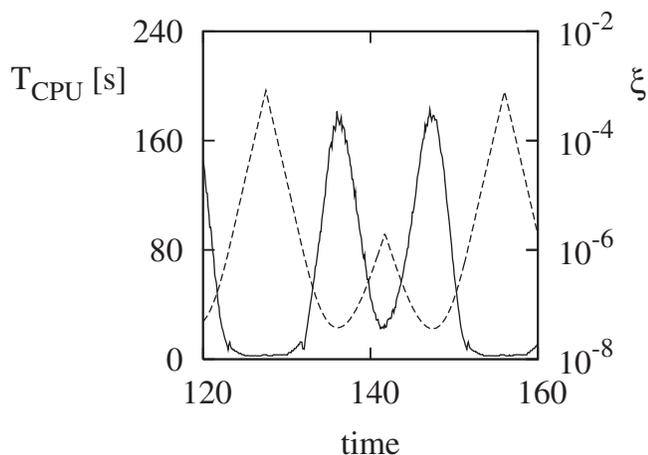

FIG. 9. Computational time of the ARK method T_{CPU} (solid line) and the smallest gap ξ given by Eq. (10) (dashed line) as functions of time for the error density per unit time $\rho = 10^{-10}$.

and Table I, we choose ρ in such a way as to obtain $\langle dt \rangle$ similar to the values used in the fixed time-step routines. In Fig. 10, the decimal logarithm of the gap between surfaces of one pair of spheres, $r_{12} - 1$, is shown as a function of time. Negative values of $r_{12} - 1$ are omitted from the plots. In Table I, also other features of the periodic trajectory are explicitly compared: The period T, the minimum value of $r_{12} - 1$ over the period ξ_{min}, and the average computational time $\langle T_{CPU} \rangle$. Additionally, it is also indicated if potential overlaps have been detected during the integration and treated by the corresponding overlap-avoiding procedure. Notice that in the case of radius renormalization methods, when the spheres are allowed to overlap, ξ_{min} becomes negative.

As seen in Fig. 10 and Table I, there are significant, both quantitative and qualitative, differences between the results obtained by different methods, which will now be discussed in detail. A striking feature of IEC trajectory in Fig. 10 is the presence of long chains of collisions, corresponding to non-smooth parts of the plots. This shows, surprisingly, that single collisions are rare. The effect of collisions is the most significant in the IEC procedure; actually, the collisions change the dynamics of very close particles in a profound way. In the case of the IE scheme, paradoxically, the collisions induce the tendency of particles to stay together longer and at smaller distances than the ones calculated by the reference fourth order ARK scheme.[34] Decreasing the time step in IEC procedure, we observe that the period of the motion is constantly increasing, whereas minimal distance between the sphere surfaces is decreasing, reaching the numerical noise level at $dt = 0.001$. Therefore, IEC routine does not seem to converge. Moreover, the results of IEC method differ from the benchmark solution. For the IEC scheme with the smallest time step $dt = 0.001$, the period is $T = 209$ and the minimal distance between the sphere surfaces $r_{min} = 5 \times 10^{-15}$. For the benchmark solution, the period and the minimal distance between the sphere surfaces are $T = 170$ and $r_{min} = 3 \times 10^{-8}$, respectively.

In the solution obtained by the IER routine, the particles overlap most of the time, as illustrated in Fig. 10. The period is about 50% larger than that in the case of the benchmark motion and does not seem to converge to the proper limit with decreasing time step. Moreover, the depth of the overlap significantly increases with time, as seen in Fig. 11. Summarizing, both IEC and IER procedures fail to reproduce the benchmark solution.

Contrary to the IE procedures, both the Adams–Bashforth and fixed time Runge–Kutta integration methods do converge and are able to reproduce the benchmark solution for sufficiently small time step, as indicated in Fig. 10 and Table I. Such a result is to be expected because for $dt \leq 0.001$, no potential overlap has been detected and, therefore, not a single event of radius renormalization or elastic collision has occurred.

Comparing accuracy of the overlap-avoiding procedures, based on Table I and Fig. 10, naturally, we need to concentrate on time steps large enough for overlaps to occur, i.e., on $dt = 0.1$ and $dt = 0.01$ (and the corresponding values of $\langle dt \rangle$ for ARK). Analyzing trajectories evaluated with the time step $dt = 0.1$, we conclude that too large time steps of the ABC,
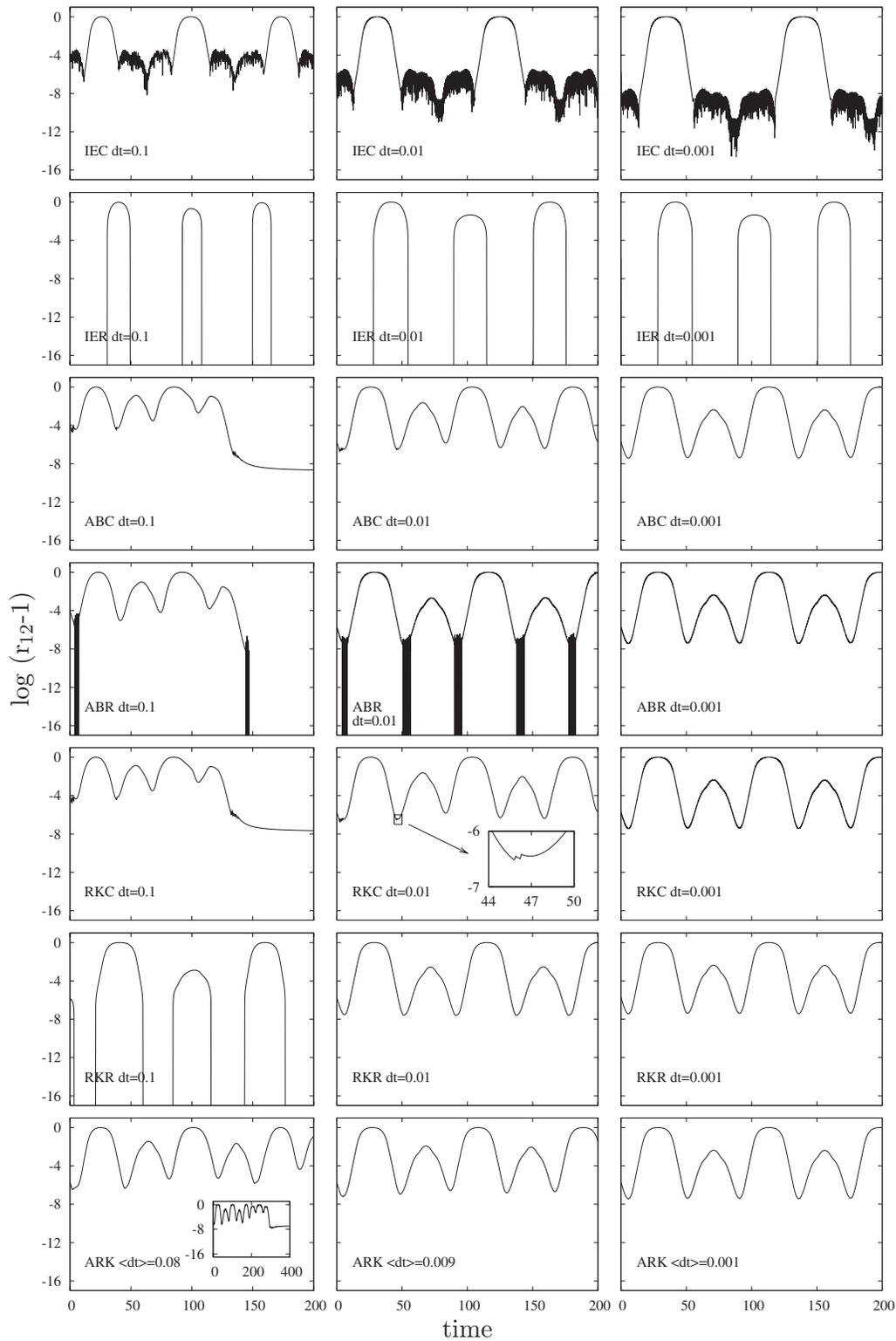
FIG. 10. The gap between surfaces of two spheres, labeled 1 and 2, as a function of time, obtained with the use of different integration routines and methods of treating overlaps.

ABR, RKC, and ARK procedures lead to separation of the group of particles, with a single particle left behind a faster pair, after approximately one period of the butterfly trajectory. The computed evolution is therefore qualitatively different from the benchmark periodic settling. On the other hand, for the RKR method with $dt=0.1$, the motion remains

periodic up to at least $10^3\tau_s$, although the period of the motion is significantly larger than that of the benchmark solution.

Much better results are obtained with smaller time steps, e.g., $dt=0.01$. The AB method has a similar accuracy as the RK procedure, but it is about five times faster (since it uses

TABLE I. Comparison of accuracy and efficiency of different integration routines and methods of treating overlaps.

		Time step	T	ξ_{min}	$\langle T_{CPU} \rangle$ (s)	Overlaps
IEC		$dt=0.1$	151	4.0×10^{-11}	0.85	Yes
		$dt=0.01$	186	4.6×10^{-13}	3.25	Yes
		$dt=0.001$	209	5.8×10^{-15}	19.1	Yes
IER		$dt=0.1$	235	-0.74	0.46	Yes
		$dt=0.01$	243	-0.05	2.02	Yes
		$dt=0.001$	245	3.5×10^{-8}	18.9	Yes
ABC		$dt=0.1$	132	1.6×10^{-9}	0.109	Yes
		$dt=0.01$	155	2.1×10^{-7}	1.05	Yes
		$dt=0.001$	170	3.5×10^{-8}	10.2	No
ABR		$dt=0.1$	137	-4.3×10^{-5}	0.108	Yes
		$dt=0.01$	174	-3.6×10^{-7}	1.04	Yes
		$dt=0.001$	170	3.5×10^{-8}	10.2	No
RKC		$dt=0.1$	132	1.7×10^{-8}	0.58	Yes
		$dt=0.01$	155	2.1×10^{-7}	5.75	Yes
		$dt=0.001$	170	3.5×10^{-8}	52.9	No
RKR		$dt=0.1$	238	-9.8×10^{-6}	0.58	Yes
		$dt=0.01$	172	2.5×10^{-8}	5.5	Yes
		$dt=0.001$	170	3.5×10^{-8}	52.6	No
ARK	$\rho=10^{-1}$	$\langle dt \rangle \approx 0.081$	147	2.8×10^{-8}	0.7	Yes
	$\rho=10^{-6}$	$\langle dt \rangle \approx 0.009$	162	6.4×10^{-8}	1.6	No
Benchmark	$\boldsymbol{\rho=10^{-10}}$	$\boldsymbol{\langle dt \rangle \approx 0.001}$	**170**	$\boldsymbol{3.5 \times 10^{-8}}$	**17.1**	**No**

only one mobility matrix computation per time step, in contrast to RK, which needs five such computations). When the elastic collisions are used to avoid overlaps, the integration with AB and RK routines gives nearly indistinguishable results, as seen in Fig. 10 and in the top panel of Fig. 12. However, in the case of the radius renormalization, RK seems to perform better than AB since it avoids sequences of
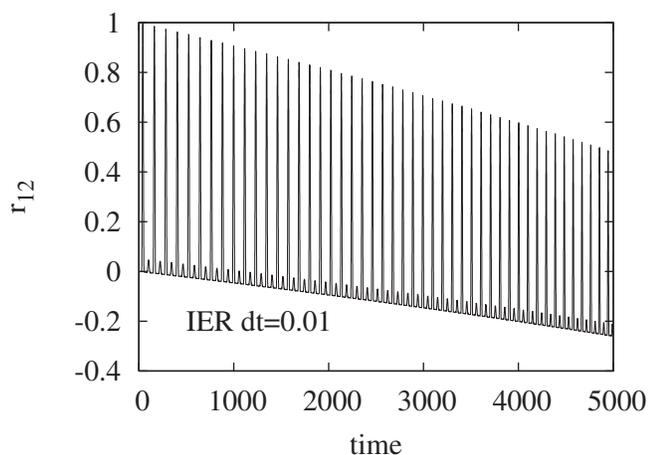

FIG. 11. Time dependence of the gap between the surfaces of particles 1 and 2, evaluated by the IER procedure. Negative values correspond to the particle overlap.
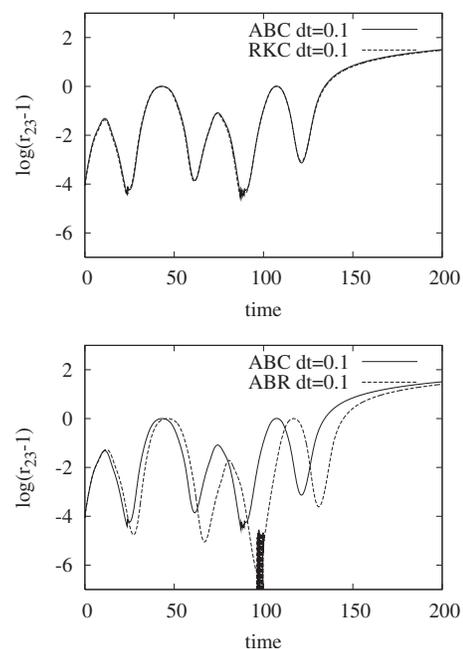

FIG. 12. Time dependence of the gap between the surfaces of particles 2 and 3. The choice of the integration routine (top panel) has a less significant impact on the solution than the choice of the overlap-avoiding procedure (bottom panel).

oscillations between negative and positive values of the gap, visible as thick black vertical lines in Fig. 10. Such sequences has also been reported in an ABR method applied in Ref. 17 to simulations of sheared hard-sphere suspensions.

Interestingly, the choice of the overlap-avoiding procedure seems to have a greater impact on the trajectories than the choice of the integration scheme, as may be concluded from the comparison of the bottom panel of Fig. 12, where the results of ABC and ABR are plotted together, with the top one, where the results of ABC and RKC are plotted together.

In comparison with the fixed time step routines (AB and RK), the adaptive ARK method with the comparable averaged time-step is surprisingly efficient, being more than three times faster than RK and only about 50% slower than AB.

Summarizing, for our benchmark trajectory, the best choice of the integrating routine seems to be either any of the radius renormalization procedures (RKR or ABR) or the ARK method with additional time-step division if the potential overlap is detected. The best accuracy can be obtained by the RKR procedure with sufficiently small time steps (for $dt=0.01$, the period of the motion is computed with the accuracy of 1%). On the other hand, if computational speed is a main concern, then one can choose the ABR or ARK method. The first of them, ABR, is the fastest and gives 2% accuracy of the period (for $dt=0.01$) but leads to unphysical oscillations between the positive and negative values of the gap size. The second one, ARK with a comparable averaged time step, results in 5% precision of the period and is only 50% slower than ABR.

Generalization of these conclusions for other systems should be treated with caution because for our benchmark trajectory, the sliding motion plays the most prominent role. Especially at the smallest gaps between the particle surfaces, where the potential overlaps are detected, the sliding velocity is many orders of magnitude larger than the shearing one. It is not clear if this feature is indeed generic for all the potential overlaps. Also, the presence of the external shear flow may lead to additional complications.[17]

VI. CONCLUSIONS

In this study, we considered the dynamics of close spherical particles moving in a viscous fluid. A benchmark periodic trajectory of three spheres was found, with the particles remaining constantly within a very short distance to each other. The period of the motion corresponds to about $170\tau_s$ (85 Stokes times), and the longest simulations reported reached more than 100 periods. Most of the time, the particles are in a sliding motion relative to each other, followed by rapid changes of direction of the relative motion. The smallest gap between the particles constantly remains below 1% of their diameter. This is in contrast to previously reported trajectories that mostly have a scattering character, i.e., particles drift away from each other after some short-distance interaction. Permanent proximity of the particles makes the considered trajectory an ideal benchmark for comparisons of accuracy between different numerical methods. In particular, it is possible to test different approaches to the

problem of the particle overlaps that are numerical artifacts of most fixed time-step integrating routines. The results of our analysis show that the details of the particle motion strongly depend on both the method used to integrate the equations of motion and the method used to avoid the overlaps.

For sufficiently small time–steps, the Runge-Kutta and Adams–Bashforth fixed-time integration routines give reasonable results, if combined with the radius renormalization or elastic collisions as the overlap-avoiding procedures. Also, the adaptive Runge–Kutta scheme with additional time-step division performs well. For our benchmark trajectory and a given time step, the best accuracy is obtained by the fixed-time Runge–Kutta method with the radius renormalization, RKR, which also allows for the largest time-steps. On the other hand, the fastest is the AB procedure with the radius renormalization, ABR, which evaluates the period with a comparable precision to RKR but leads to a large number of oscillations between positive and negative values of the gap that separates the particles' surfaces. Alternatively, one can use the adaptive Runge–Kutta method with the additional time-step reduction in the case of potential overlaps, ARK, which produces acceptable accuracy with reasonable speed.

APPENDIX A: ERROR CALCULATION IN ADAPTIVE RUNGE–KUTTA METHOD

In this appendix, we discuss the accuracy of the adaptive Runge–Kutta algorithm, following Ref. 36. A good estimate of a truncation error of the algorithm is

$$\Delta_1(dt) = \sqrt{\sum_{i=1}^{3} |\mathbf{r}_i^{(5)}(t+dt) - \mathbf{r}_i^{(4)}(t+dt)|^2}, \qquad \text{(A1)}$$

where $|\mathbf{r}_i^{(5)}(t+dt) - \mathbf{r}_i^{(4)}(t+dt)|$ is the difference between fifth order and fourth order Runge–Kutta results for the position of particle i at the next time step dt. This error is then compared to the desired accuracy Δ_0,

$$\Delta_0(dt) = \rho dt, \qquad \text{(A2)}$$

where ρ is the error density per unit time, specified at the beginning of the simulation. A new value of the time step dt' is then calculated as[36]

$$dt' = \begin{cases} Sdt \left| \dfrac{\Delta_0}{\Delta_1} \right|^{1/5} & \text{if } \Delta_0 \geq \Delta_1 \\[2ex] Sdt \left| \dfrac{\Delta_0}{\Delta_1} \right|^{1/4} & \text{if } \Delta_0 < \Delta_1, \end{cases} \qquad (A3)$$

where we take the safety factor S equal to 0.95.

APPENDIX B: IMPLICIT AND EXPLICIT EULER METHOD WITH COLLISIONS

As described in Sec. III, the explicit Euler method with hard-sphere collisions may be represented formally as

$$\mathbf{X}(t+dt) = \mathbf{X}(t) + \{\mathbf{V}[\mathbf{X}(t)]dt\}_{\text{HS}} \qquad (B1)$$

where an index HS means that a hard-sphere dynamics is used to advance the system by dt. In the above equation, the particle velocities are computed at the beginning of the time step, just as in any explicit (forward) Euler method. However, explicit Euler method suffers from numerical instability problem and one needs to resort to impractically short time steps to obtain reliable results. To avoid this problem, the following implicit scheme may be used:

$$\mathbf{X}(t+dt) = \mathbf{X}(t) + \{\mathbf{V}[\mathbf{X}(t+dt)]dt\}_{\text{HS}}, \qquad (B2)$$

which we are going to call "implicit Euler method with collisions" (IEC). To find $\mathbf{X}(t+dt)$, we use a fixed point iteration scheme, with an initial guess $\mathbf{X}^0(t+dt)=\mathbf{X}(t)$. The iterations are stopped when the difference between the values of $\mathbf{X}(t+dt)$ calculated in successive iterations is smaller than 10^{-5}.

[1] S. Kim and S. J. Karrila, *Microhydrodynamics: Principles and Selected Applications* (Butterworth-Heinemann, London, 1991).

[2] J. Happel and H. Brenner, *Low Reynolds Number Hydrodynamics* (Noordhoff, Leyden, 1973).

[3] A. J. C. Ladd, "Numerical simulations of particulate suspensions via a discretized Boltzmann equation," J. Fluid Mech. **271**, 285 (1994).

[4] J. F. Brady and G. Bossis, "Stokesian dynamics," Annu. Rev. Fluid Mech. **20**, 111 (1988).

[5] B. Cichocki, B. U. Felderhof, K. Hinsen, E. Wajnryb, and J. Bławdziewicz, "Friction and mobility of many spheres in Stokes flow," J. Chem. Phys. **100**, 3780 (1994).

[6] D. J. Jeffrey and Y. Onishi, "The forces and couples acting on two nearly touching spheres in low-reynolds-number flow," ZAMP **35**, 634 (1984).

[7] G. Bossis and J. F. Brady, "Dynamic simulation of sheared suspensions. I. General method," J. Chem. Phys. **80**, 5141 (1984).

[8] A. J. C. Ladd, "Dynamical simulations of sedimenting spheres," Phys. Fluids A **5**, 299 (1993).

[9] A. Sierou and J. F. Brady, "Shear-induced self-diffusion in non-colloidal suspensions," J. Fluid Mech. **506**, 285 (2004).

[10] R. C. Ball and J. R. Melrose, "Lubrication breakdown in hydrodynamic simulations of concentrated colloids," Adv. Colloid Interface Sci. **59**, 19 (1995).

[11] R. C. Ball and J. R. Melrose, "A simulation technique for many spheres in quasi-static motion under frame-invariant pair drag and Brownian forces," Physica A **247**, 444 (1997).

[12] S. L. Dance, E. Climent, and M. R. Maxey, "Collision barrier effects on the bulk flow in a random suspension," Phys. Fluids **16**, 828 (2004).

[13] D. I. Dratler, W. R. Schowalter, and R. L. Hoffman, "Dynamic simulation of shear thickening in concentrated colloidal suspensions," J. Fluid Mech. **353**, 1 (1997).

[14] R. H. Davis, "Effects of surface roughness on a sphere sedimenting through a dilute suspension neutrally buoyant spheres," Phys. Fluids A **4**, 2607 (1992).

[15] M. L. Ekiel-Jeżewska, F. Feuillebois, N. Lecoq, K. Masmoudi, R. Anthore, F. Bostel, and E. Wajnryb, "Hydrodynamic interactions between two spheres at contact," Phys. Rev. E **59**, 3182 (1999).

[16] M. L. Ekiel-Jeżewska and E. Wajnryb, "Equilibria for the relative motion of three heavy spheres in Stokes fluid flow," Phys. Rev. E **73**, 046309 (2006).

[17] D. I. Dratler and W. R. Schowalter, "Dynamic simulation of suspensions of non-Brownian hard spheres," J. Fluid Mech. **325**, 53 (1996).

[18] B. Cichocki, M. L. Ekiel-Jeżewska, and E. Wajnryb, "Lubrication corrections for three-particle contribution to short-time self-diffusion coefficients in colloidal dispersions," J. Chem. Phys. **111**, 3265 (1999).

[19] B. U. Felderhof, "Many-body hydrodynamic interactions in suspensions," Physica A **151**, 1 (1988).

[20] G. Drazer, J. Koplik, B. Khusid, and A. Acrivos, "Deterministic and stochastic behaviour of non-Brownian spheres in sheared suspensions," J. Fluid Mech. **460**, 307 (2002).

[21] G. Bossis and J. F. Brady, "Dynamic simulation of sheared suspensions. I. General method," J. Chem. Phys. **80**, 5141 (1984).

[22] B. J. Alder and T. E. Wainwright, "Studies in molecular dynamics. II. behavior of a small number of elastic spheres," J. Chem. Phys. **33**, 1439 (1960).

[23] K. O. L. F. Jayaweera, B. J. Mason, and G. W. Slack, "The behaviour of clusters of spheres falling in a viscous fluid. Part 1. Experiment," J. Fluid Mech. **20**, 121 (1964).

[24] L. M. Hocking, "The behaviour of clusters of spheres falling in a viscous fluid. Part 2. Slow motion theory," J. Fluid Mech. **20**, 129 (1964).

[25] I. M. Jánosi, T. Tél, D. E. Wolf, and J. A. C. Gallas, "Chaotic particle dynamics in viscous flows: The three-particle Stokeslet problem," Phys. Rev. E **56**, 2858 (1997).

[26] M. Golubitsky, M. Krupa, and C. Lim, "Time-reversibility and particle sedimentation," SIAM J. Appl. Math. **51**, 49 (1991).

[27] R. E. Caflisch, C. Lim, J. H. C. Luke, and A. S. Sangani, "Periodic solutions for three sedimenting spheres," Phys. Fluids **31**, 3175 (1988).

[28] E. J. Hinch, in *Disorder and Mixing*, edited by E. Guyon, J.-P. Nadal, and Y. Pomeau (Kluwer, Dordrecht, 1988), pp. 153–161.

[29] G. I. Taylor, *Low Reynolds Number Flow* (Encyclopaedia Britannica Educational Corp., Chicago, 1967).

[30] C. Moore, "Braids in classical dynamics," Phys. Rev. Lett. **70**, 3675 (1993).

[31] A. Chenciner and R. Montgomery, "A remarkable periodic solution of the three body problem in the case of equal masses," Ann. Math. **152**, 881 (2000).

[32] R. Montgomery, "A new solution to the three-body problem," Not. Am. Math. Soc. **48**, 471 (2001).

[33] At the minimum of r_{23}, reached at $t=t_m$, obviously $v_n/v_t=0$. Close to the minimum, for $t_m-T/36 < t < t_m+T/36$, the ratio of the corresponding velocity components, v_n/v_t, is smaller than 3×10^{-5}. This is the only time interval when the minimal gap size stays below 10^{-6}.

[34] The unphysical tendency of the IEC procedure to "glue" the particles together actually helped us to find the family of butterfly periodic and quasi-periodic trajectories.

[35] W. Humphrey, A. Dalke, and K. Schulten, "VMD—Visual molecular dynamics," J. Mol. Graphics **14**, 33 (1996).

[36] W. H. Press, B. P. Flannery, S. A. Teukolsky, and W. T. Vetterling, *Numerical Recipes: The Art of Scientific Computing*, 2nd ed. (Cambridge University Press, Cambridge 1992).